GSA DATA REPOSITORY 2014347

"Seismically active sub-crustal magma source of the Klyuchevskoy volcano in Kamchatka"

By Levin, Droznina, Gavrilenko, Carr, Senyukov.

Supplementary Material

1. Constraints on the crustal structure from receiver function analysis.

1.1 Data.

We use records of distant (teleseismic) earthquakes recorded by a set of continuously operating digital seismic stations (Figures 1, 3 of the main text, and figures S1 and S2). These include permanent observatories operated by Kamchatka Branch of the Geophysical Service (KBGS) and a portable deployment carried out jointly by the University of Alaska and KBGS. Specifically, sites KLY, KRS, KMN and LGN are operated by KBGS, their coordinates and recording parameters can be found at http://emsd.ru/rtss/stations (the site is in Russian). For the analysis presented in this study we used teleseismic earthquake records from sites KLY, KRS and KMN recorded between 2005 and 2012. As these are remote sites operating in harsh conditions, data are available at each for a subset of time interval. Data from these sites were provided for the purpose of the collaborative research in accordance with a bilateral agreement between KBGS and Rutgers University. Stations BESA, BESD, BERG, BEZE and BELO were deployed for different periods of time between the summer of 2007 and the fall of 2010. Information about these stations, including the availability of their data, is at http://www.iris.edu/gmap/YC?timewindow=2006-2010.

1.2 Earthquake size measures.

The measure of earthquake size adopted in Russian literature is called an "energy class". It is philosophically similar to the more common magnitude (cf. Rautian et al., 2007). A relationship between the energy class K_S and the local magnitude M_L calibrated for Kamchatka is $M_L = \frac{K_S}{2} - 0.75$ (Senyukov et al., 2009).

1.3 Appearance and timing of P-to-S converted waves.

Phases present in receiver function time series may be used to evaluate the depth to the converting boundary provided the nature of these phases is properly interpreted. A subhorizontal converting boundary should give rise to a P-to-S phase for waves arriving at the same time from all directions. Thus for a first check we construct backazimuth gathers of receiver functions and identify phases that are present from a significant fraction of the back-azimuthal range. Furthermore, delays of direct P-to-S converted waves that traverse the crust only once are expected to decrease with an increase of source distance.

For phases that traverse the crust more than once this delay is expected to grow. We examine the changes of delay with source distance (the “moveout”) of target phases in epicentral gathers of receiver functions. Figures S1 and S2 show both types of receiver function gathers.

Computation of receiver functions is carried out using a multi-taper spectral coherence algorithm of Park and Levin (2000). Data are grouped into bins 15° in backazimuth and 10° in the epicentral distance, with 50% overlap. Epicentral gathers are constructed for the 140°-270° backazimuth range that contains most of the events observed. The range of frequencies in the timeseries is limited to 0.5 Hz and lower.

Receiver function timeseries have “positive” values when P-to-S converted wave is of the same polarity as the parent P wave. When seismic velocity increases with depth (e.g., at the crust-mantle boundary) a positive P-to-S converted wave is expected. Consequently, in our examination of the receiver functions we focus on the positive phases. Attributes (directional consistency, correct moveout) of two such phases, at ~3 s and ~6 s delays, in most receiver function gathers give us confidence that these are indeed up-going P-to-SV converted waves originating from sub-horizontal impedance contrasts at depth.

1.4 Constraints on the depth to the crust-mantle boundary and the properties of the crustal material.

Receiver function time series contain both direct P-to-S converted waves and waves that reverberate in the crust. Relative timing of these different converted phases may be predicted if the crustal thickness (H), the Vp/Vs ratio (k), and either Vp or Vs are known. For a choice of H and k values a sum of weighted receiver function amplitudes at the times when converted phases are expected is large if the prediction corresponds to

timing of the observed phases, and amplitudes add constructively. It is small if the predicted times “miss” the observed phases. A search over possible ranges of H and k values offers a means to assess likely combinations of these parameters that best match the data (Zhu and Kanamori, 2000). Plots of resulting stacked amplitude surfaces are presented in the lower rows of figures S1 and S2, showing characteristic trade-offs in values of H and k.

At all sites H-k stacking surfaces display multiple maxima suggesting complex crustal and upper mantle structure. Sites closest to Klyuchevskoy show largest stack energy for crustal thickness 26-28.5 km, sites further away (KRS and KMN) have largest energy at depth 42.5 and 47.5 km, while at site KLY the largest stacking amplitude corresponds to a boundary at ~15 km. All values are contingent on the choice of the Vp=6.1 km/s used in the earthquake location model (Figure S3). It should be noted that in all plots shapes of the shaded regions correspond to the expected stack surface patterns of the direct P_S converted wave, while trends typical of the reverberations that are expected to intersect this pattern are not obvious. Complexity of the crustal structure is a likely cause of the low coherence in reverberating waves. This limits the confidence of the constraints on k, as the tradeoff patters show similar amplitude over broad ranges.

2. Constraints on the depth of melting beneath Klyuchevskoy.

2.1 Klyuchevskoy parental melts barometry.

We used the thermobarometer developed by Lee et al. (2009) to estimate the melting pressures beneath Klyuchevskoy volcano. The barometer is based on Si activity in parental melts saturated with orthopyroxene and olivine, utilizing major element concentrations, water concentrations and Fe^{3+}/Fe^{total} estimates.

Portnyagin et al. (2007) report 29 compositions of melt inclusions trapped in primitive olivines (Fo# from 79.4 to 90.6) from Klyuchevskoy. In order to infer the parental melts we picked 9 compositions which were trapped in the most magnesian olivine crystals (Fo# from 89.2 to 90.6). Mironov and Portnyagin (2011) assume that Klyuchevskoi's parental melts are in equilibrium with olivine Fo_{91}. In order to assess compositions of near primary melts we added equilibrium olivine to the melt inclusions incrementally (using Fe^{3+}/Fe^{total} = 0.15; and K_D=0.32 for the Fe^{2+}/Mg exchange) until the melt is in equilibrium with Fo_{91}. For the H_2O content, we use the estimation (3.5 wt.%) from Mironov and Portnyagin (2011).

In addition to the melt inclusions we used the most primitive Klyuchevskoy lava , sample KL-3 from Almeev et al. (2013). We used PRIMACAL2 software developed by Kimura and Ariskin (2014) based on reverse crystallization combined with forward modeling in order to infer a parental melt composition from KL-3.

The Lee et al. (2009) barometer has an uncertainty ± 0.2 GPa or about 7 km of depth. Adding 1.0 wt % water decreases the depth estimate by 0.7 km, so error related to water content is negligible. Increasing the oxygen fugacity from QFM to NNO reduces estimated depths by about 3.5 km.

We report all obtained Klyuchevskoy parental melt compositions (9 from the melt inclusions, 1 from the most primitive lava) and the melting P and T conditions in the supplement table S1.

2.2 Klyuchevskoy magma crystallization depth estimation based on olivine and clinopyroxene simultaneous crystallization.

The most primitive Klyuchevskoy lava, sample KL-3 from Almeev et al. (2013), has MgO = 12.1 wt.%) and contains almost equal amounts of olivine and clinopyroxene phenocrysts; Ol – 8,5 vol.%, Cpx – 9.1 vol.%. Assuming that olivine and clinopyroxene crystallized together we estimate the crystallization pressure following Danyushevsky et

al. (1996). The method relies on the fact that pressure increases the crystallization temperature of clinopyroxene much more than the crystallization temperature of olivine. Thus, the higher the pressure the earlier clinopyroxene appears on the liquidus. The greater the difference between the calculated 1 atm crystallization temperatures for olivine and clinopyroxene the greater the crystallization pressure.

We used two different software packages for modeling: PETROLOG ver. 3.1.1.3 (Danyushevsky and Plechov, 2011) and COMAGMAT ver. 3.72 (Ariskin et al., 1993; Ariskin and Barmina, 2004) to model the most primitive Klyuchevskoy lava composition (sample KL-3). We assumed a magma water content of 3.5 wt.% (Mironov and Portnyagin, 2011) and allowed the liquidus temperature to reflect the effect of water following Danyushevsky (2001) for PETROLOG and Almeev et al. (2007) for COMAGMAT.

We obtained these results:

PETROLOG ver. 3.1.1.3 – 12.0 kbar, 1244^{o}C
COMAGMAT ver. 3.72 – 12.1 kbar, 1235^{o}C

2.3 Klyuchevskoy magma crystallization depth estimation based on volatiles content.

From melt inclusion studies Mironov and Portnyagin (2011) estimated the volatile content of Klyuchevskoy parental melts (CO_2 = 0.9 wt.%, H_2O = 3.5 wt.%). From this data they estimated formation depths of Klyuchevskoy primary melts at 30-40 km. According to recent experimental data (Shishkina, 2012) this CO_2 content corresponds to pressures in excess of 900 MPa.

References:

Almeev, R.R., Holtz, F., Koepke, J., Parat, F., and Botcharnikov, R.E., 2007, The effect of H_2O on olivine crystallization in MORB: Experimental calibration at 200 MPa: American Mineralogist, v. 92, no. 4, p. 670-674. doi: 10.2138/am.2007.2484

Almeev, R.R., Kimura, J.I., Ariskin, A.A., and Ozerov, A.Y., 2013, Decoding crystal fractionation in calc-alkaline magmas from the Bezymianny Volcano (Kamchatka, Russia) using mineral and bulk rock compositions: Journal of Volcanology and Geothermal Research, v. 263, p. 141-171. doi: 10.1016/j.jvolgeores.2013.01.003

Ariskin, A.A., and Barmina, G.S., 2004, COMAGMAT: Development of a magma crystallization model and its petrological Applications: Geochemistry International, v. 42, p. S1-S157.

Ariskin, A.A., Frenkel, M.Y., Barmina, G.S., and Nielsen, R.L., 1993, COMAGMAT: a Fortran program to model magma differentiation processes: Computers & Geosciences, v. 19, no. 8, p. 1155-1170. doi: 10.1016/0098-3004(93)90020-6

Danyushevsky, L.V., 2001, The effect of small amounts of H2O on crystallisation of mid-ocean ridge and backarc basin magmas: Journal of Volcanology and Geothermal Research, v. 110, no. 3–4, p. 265-280. doi: 10.1016/0098-3004(93)90020-6

Danyushevsky, L.V., and Plechov, P., 2011, Petrolog3: Integrated software for modeling crystallization processes: Geochemistry Geophysics Geosystems, v. 12, no. 7. 10.1029/2011gc003516

Danyushevsky, L.V., Sobolev, A.V., and Dmitriev, L.V., 1996, Estimation of the pressure of crystallization and H2O content of MORB and BABB glasses: calibration of an empirical technique: Mineralogy and Petrology, v. 57, no. 3-4, p. 185-204. doi: 10.1007/BF01162358

Fedotov, S.A., Zharinov, N.A., and Gontovaya, L.I., 2010, The magmatic system of the Klyuchevskaya group of volcanoes inferred from data on its eruptions, earthquakes, deformation, and deep structure: Journal of Volcanology and Seismology, v. 4, no. 1, p. 1-33. doi: 10.1134/S074204631001001X

Kimura, J.-I., and Ariskin, A.A., 2014, Calculation of water-bearing primary basalt and estimation of source mantle conditions beneath arcs: PRIMACALC2 model for WINDOWS: Geochemistry, Geophysics, Geosystems, v. 15, no. 4, p. 1494-1514. 10.1002/2014GC005329

Lee, C.-T.A., Luffi, P., Plank, T., Dalton, H., and Leeman, W.P., 2009, Constraints on the depths and temperatures of basaltic magma generation on Earth and other terrestrial planets using new thermobarometers for mafic magmas: Earth and Planetary Science Letters, v. 279, no. 1–2, p. 20-33. doi: 10.1016/j.epsl.2008.12.020

Mironov, N.L., and Portnyagin, M.V., 2011, H2O and CO2 in parental magmas of Kliuchevskoi volcano inferred from study of melt and fluid inclusions in olivine: Russian Geology and Geophysics, v. 52, no. 11, p. 1353-1367. doi: 10.1016/j.rgg.2011.10.007

Park, J., and Levin, V., 2000, Receiver Functions from Multiple-Taper Spectral Correlation Estimates: Bulletin of the Seismological Society of America, v. 90, no. 6, p. 1507-1520. doi: 10.1785/0119990122

Portnyagin, M., Hoernle, K., Plechov, P., Mironov, N., and Khubunaya, S., 2007, Constraints on mantle melting and composition and nature of slab components in volcanic arcs from volatiles (H2O, S, Cl, F) and trace elements in melt inclusions from the Kamchatka Arc: Earth and Planetary Science Letters, v. 255, no. 1-2, p. 53-69. 10.1016/j.epsl.2006.12.005

Rautian, T.G., Khalturin, V.I., Fujita, K., Mackey, K.G., and Kendall, A.D., 2007, Origins and Methodology of the Russian Energy K-Class System and Its Relationship to Magnitude Scales: Seismological Research Letters, v. 78, no. 6, p. 579-590. doi: 10.1785/gssrl.78.6.579

Senyukov, S.L., Droznina, S.Y., Nuzhdina, I.N., Garbuzova, V.T., and Kozhevnikova, T.Y., 2009, Studies in the activity of Klyuchevskoi volcano by remote sensing techniques between January 1, 2001 and July 31, 2005: Journal of Volcanology and Seismology, v. 3, no. 3, p. 191-199. doi: 10.1134/S0742046309030051

Shapiro, N.M., Gorbatov, A.V., Gordeev, E., and Dominguez, J., 2000, Average shear-wave velocity structure of the Kamchatka peninsula from the dispersion of surface waves: Earth, Planets and Space, v. 52, no. 9, p. 573-577. doi: 10.1186/BF03351665

Shishkina, T.A., 2012, Storage conditions and degassing processes of low-K and high-Al tholeiitic island-arc magmas: experimental constraints and natural observations for Mutnovsky volcano, Kamchatka, Ph.D.: Leibniz Universität Hannover, 214 p.

Zhu, L., and Kanamori, H., 2000, Moho depth variation in southern California from teleseismic receiver functions: Journal of Geophysical Research: Solid Earth, v. 105, no. B2, p. 2969-2980. doi: 10.1029/1999JB900322

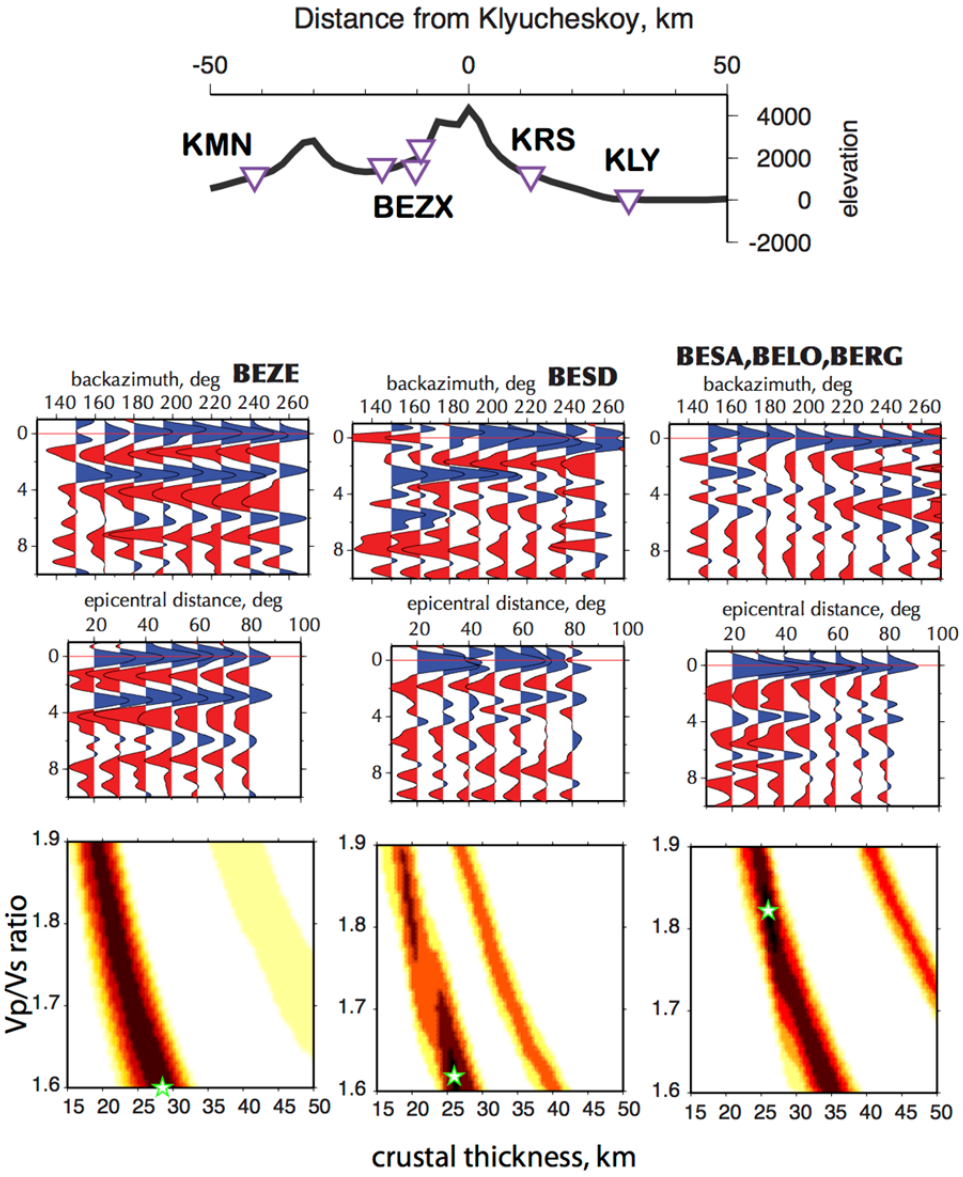

Figure DR1. Receiver functions and H-k stacking error surfaces for seismic stations in the vicinity of the Bezymiany volcano, presented in the form of backazimuth (top row) and epicentral (middle row) gathers, and results of stacking the amplitudes of direct and multiply-reflected waves according to the prediction from combinations of crustal thickness and Vp/Vs ratio (bottom row). Positive phases on receiver functions are shaded blue. H-k stack surfaces are shaded progressively darker colors for larger values, with a global maximum of the entire surface shown by the star. Locations of the seismic stations (triangles, upper panel) are projected onto a profile of topography along a line in Figure 1. Data from a group of nearby seismic stations on the flanks of the Bezymiany volcano (BESA,BELO, BERG) are combined into common gathers. BEZX on the upper plot marks the location of all sites near Bezymiany operated by the US-Russia collaborative PIRE project (http://www.gps.alaska.edu/PIRE/).

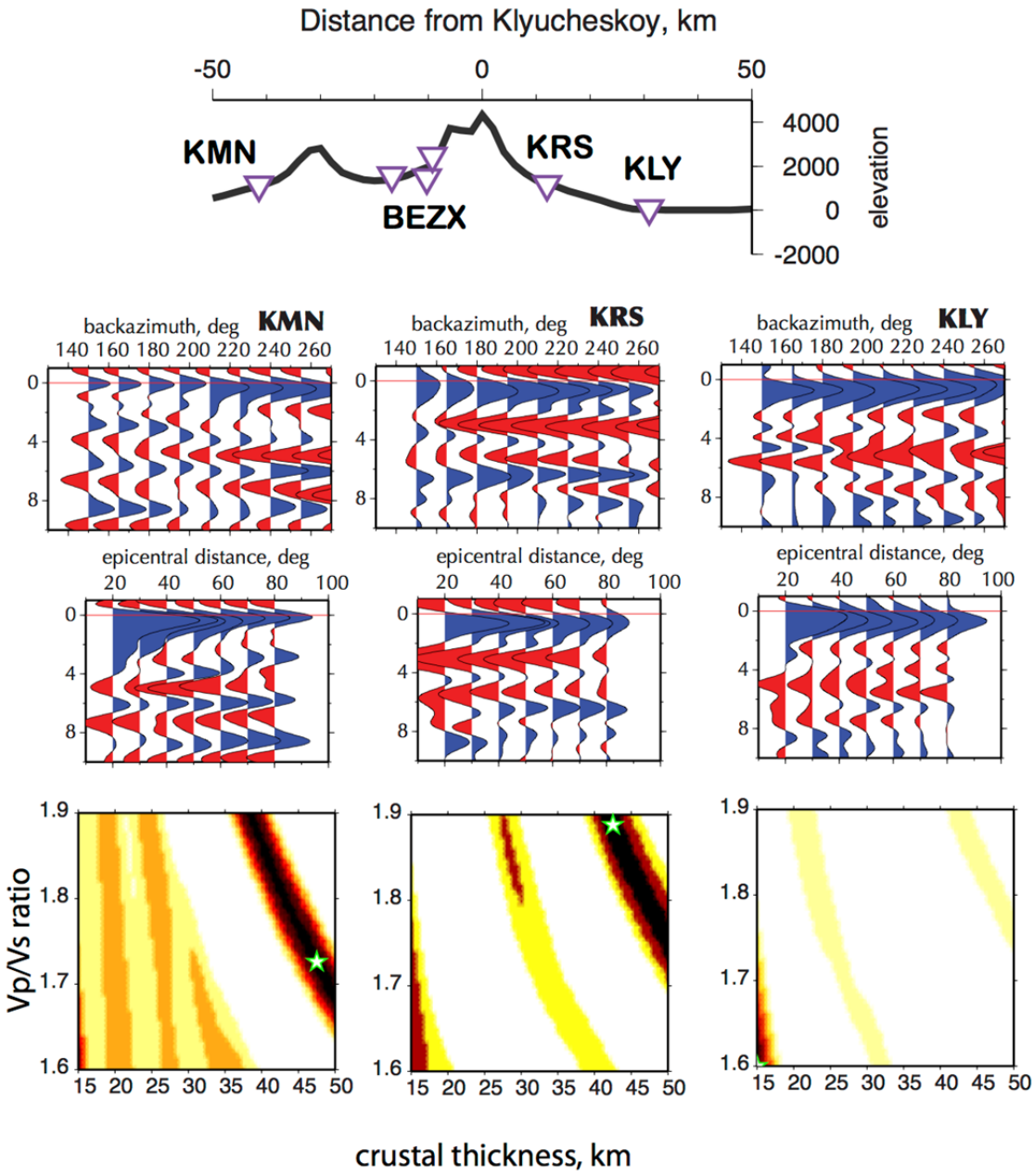

Figure DR2. Same as S1, for stations KRS, KMN and KLY operated by the Kamchatka Branch of the Geophysical Service of Russian Academy of Sciences.

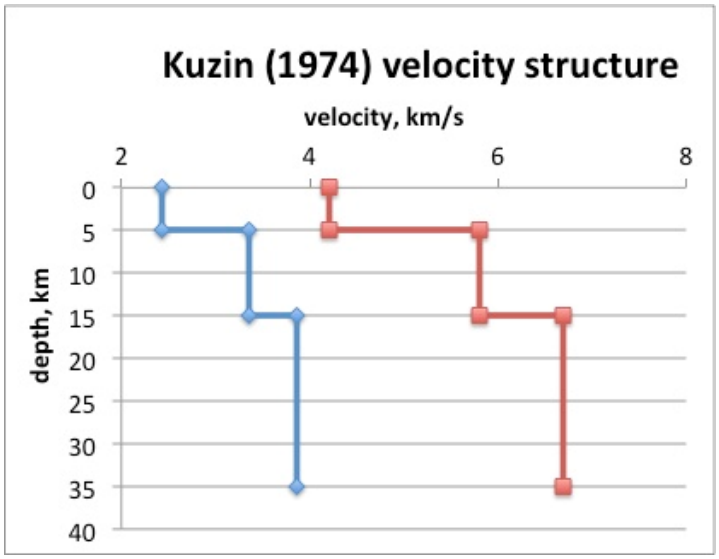

DR3. Seismic velocity profile of the crust used for earthquake locations. Depth-averaged values of this profile are also used to evaluate depths corresponding to delay times in RF time series. Values as reported in Shapiro et al. (2000).

Table DR1

Klyuchevskoy parental melts (in equilibrium with Fo91) inferred from melt inclusions (1-9) and whole rock analysis (10).

P and T values obtained using the Lee et al. (2009) thermobarometer, which has an uncertainty ± 2 kbars for pressure and ± 40 ^{o} for temperature.

Depth estimations are based on P values assuming the Klyuchevskoy crust/upper mantle densities from Fedotov et al. (2010).

	Sample name	Host olivine Fo#, mol%	SiO_2	TiO_2	Al_2O_3	FeO^{total}	MnO	MgO	CaO	Na_2O	K_2O	H_2O	T Lee, ^{o}C	P Lee, kbar	Depth, km
1	Ol20E	89.5	47.87	0.70	12.79	8.10	0.13	12.12	12.29	2.01	0.51	3.49	1277	13.4	44
2	OL23E	90.1	47.85	0.76	13.22	8.08	0.10	12.21	11.62	2.19	0.44	3.52	1278	13.7	45
3	Ol5$	89.8	48.41	0.76	13.17	8.10	0.06	12.16	10.98	2.27	0.58	3.50	1273	13.2	43
4	E288	90.1	47.19	0.76	13.50	8.27	0.10	12.55	11.53	2.21	0.38	3.51	1289	15.0	49
5	E291-2	89.6	47.17	0.71	12.88	8.28	0.08	12.55	12.56	1.96	0.35	3.46	1292	14.5	47
6	E292-1	90.6	47.23	0.73	13.39	8.25	0.09	12.59	11.61	2.20	0.38	3.54	1289	15.0	49
7	E293	89.2	47.56	0.73	13.35	8.30	0.09	12.44	11.61	2.11	0.38	3.44	1285	14.2	46
8	E296-1	89.5	45.82	0.81	14.54	8.31	0.12	12.38	11.83	2.26	0.48	3.44	1282	13.4	44
9	E320-1	89.3	48.12	0.73	12.79	8.29	0.12	12.46	11.56	2.10	0.37	3.46	1288	14.5	48
10	KL-3	-	47.62	0.73	13.35	8.31	0.11	12.54	11.25	2.31	0.36	3.42	1286	12.7	42
												Average:	**1284**	**13.9**	**46**
												Uncertainty:	40	2.0	7